RSC Advances

PAPER

View Article Online
View Journal | View Issue

Cite this: *RSC Adv.*, 2021, **11**, 34432

$NiSe/Ni_3Se_2$ on nickel foam as an ultra-high-rate HER electrocatalyst: common anion heterostructure with built-in electric field and efficient interfacial charge transfer†

Xin Ma, Jingbo Yang, Xiaoqi Xu, Hangqi Yang and Chuang Peng *

One grand challenge in green hydrogen production is to design efficient HER electrocatalysts for high-rate alkaline water electrolysis. Nickel chalcogenide coatings on nickel foam (NF) are promising HER electrocatalysts, but their high-rate performances are yet to be improved. The current work reports a $NiSe/Ni_3Se_2$@NF for alkaline HER, which requires an overpotential of only 336 mV to achieve an ultra-high current density of 1250 mA cm^{-2}, outperforming commercial Pt/C. The low onset potential of $NiSe/Ni_3Se_2$@NF is attributed to its morphology, and high surface area, as well as multiple active sites and electronic structure modulation because of the heterostructure. While these features are well-known within the current knowledge framework, new understandings are proposed on its superior high-rate performance. The common-anion feature offers abundant interfacial Ni–Se bonding and low resistance for efficient interfacial charge transfer, whereas the heterovalent-Ni-cation in the heterostructure results in a built-in electric field that further enhances the high-rate performance. This work provides new insights on both the mechanistic and methodological aspects of designing high-performance electrocatalysts operating at high current densities.

Received 16th August 2021
Accepted 18th October 2021

DOI: 10.1039/d1ra06183f

rsc.li/rsc-advances

Introduction

Water electrolysis is a key enabling technology for a sustainable hydrogen economy, because it allows facile conversion of renewable or surplus electricity to hydrogen gas, whilst contributing to the resilience and stability of the electric grid.[1,2] Commercial water electrolysis requires effective and robust electrocatalysts for efficient and high-rate hydrogen and oxygen evolution reactions (HER and OER). Alkaline water electrolysis is the most commonly used commercial technology because of its high ionic conductivity and moreover the lower OER over-potential. However, the HER in alkaline medium suffers from a higher energy barrier and poor kinetics compared with acidic solutions. Therefore, the grand challenge in HER electrocatalyst design is to achieve a low overpotential at high current densities in alkaline solutions. Platinum loaded on porous carbon (Pt/C) is the best-performing lab-scale HER electrocatalyst because of its superior catalytic activities.[3,4] Nevertheless, the most widely used commercial HER electrocatalyst is porous nickel (Ni) metal, because of its low cost, high robustness and moderate catalytic activities. The performance of Ni metal can be significantly improved by surface treatment or modification. Among others, *in situ* growth of Ni chalcogenides on Ni metal substrates is an effective and feasible method because of the facile preparation, high activity, conductivity and robustness of the chalcogenide coating.

The materials design of the Ni chalcogenide coatings includes morphological, polymorph or crystalline structure, doping, defect and heterostructure. These advanced synthetic strategies drastically improve the HER performances to even compete with the benchmark Pt/C catalyst. Among others, heterostructured Ni chalcogenides allow simultaneous incorporation of high surface area, optimized adsorption energy, enhanced intrinsic catalytic activity, large numbers and multiple active sites.[5,6] Recent studies[6,7] suggest heterostructured $NiSe/Ni_3Se_2$ on Ni foam is a highly promising HER electrocatalyst because of its optimal adsorption free energy for atomic hydrogen, Se on NiSe and Ni on Ni_3Se_2 dual active sites, and high surface area. Despite their combined merits, these $NiSe/Ni_3Se_2$ heterostructures only shows compelling HER catalytic performances at low or moderate current densities (<300 mA cm^{-2}). On the other hand, a recent phenomenon found in heterointerface, *i.e.*, built-in electric field, has been verified to increase the hydrogen yield in photocatalytic HER.[8] The presence of a built-in electric field was reported in NiS/Ni_3S_2 heterostructure,[9] which shows platinum-like catalytic behavior as a counter electrode in dye-sensitized solar cell. As a chemical

School of Resource and Environmental Sciences, Wuhan University, Wuhan 430072, P. R. China. E-mail: Chuang.peng@whu.edu.cn

† Electronic supplementary information (ESI) available. See DOI: 10.1039/d1ra06183f

and structural analogue of NiS/Ni_3S_2, $NiSe/Ni_3Se_2$ heterostructure is also expected to yield a built-in electric field that can boost its HER performances at high current densities. Although this hypothesis is highly plausible, it has not verified so far, because there is still a lack of both experimental evidence and design principles for such heterostructure with high-rate HER behaviour. We herein report a common-anion heterovalent-Ni-cation type $NiSe/Ni_3Se_2$ heterostructure on Ni foam by one-step hydrothermal synthesis. This rationally designed electrode shows lower overpotential compared with Pt/C at ultra-high current densities up to 1.25 A cm^{-2}. Furthermore, we propose the general rules on optimal heterostructure design for HER, particularly the synergistic effects of intrinsic activity, site exposure and built-in electric field.

Results and discussion

Two single-phase nickel selenide coating on nickel foam, NiSe@NF and Ni_3Se_2@NF, heterostructured $NiSe/Ni_3Se_2$@NF, and dissimilar-anion heterostructured $NiSe/Ni_3S_2$@NF were prepared by one-step solvothermal process (details in the Experimental section of the ESI†). SEM images (Fig. 1) show that all the four samples have similar morphologies of uniform 1D nanorod arrays on the nickel substrate, though the sizes, shape and lengths show variations. It is also observed that the nanorods of $NiSe/Ni_3Se_2$@NF has a comparatively rougher surface than the other three samples. For all four samples, the nanorods are near-vertically grown on NF, with diameters between 200 and 500 nm and lengths of several micrometers. Electrodes with such nanorod arrays on the surfaces are highly desired because of the increased number of active sites and improved electrolyte accessibility. Moreover, this sub-micrometer-scale architecture commonly generates a hydrophilic and aerophobic surface that leads to enhanced mass transfer during gas evolving reaction.[10] The contact angles with water droplet and air bubble (Fig. S1†) indeed suggest that $NiSe/Ni_3Se_2$@NF is much more hydrophilic and slightly more aerophobic than bare NF. The powder X-ray diffraction (XRD) patterns (Fig. 2a) indicates single phase NiSe (JCPDS no. 75-0610 and JCPDS no. 29-0935) and Ni_3Se_2 (JCPDS no. 19-0841) structures of NiSe@NF and Ni_3Se_2@NF. In contrast, the XRD patterns of the two heterostructures, $NiSe/Ni_3Se_2$@NF, and $NiSe/Ni_3S_2$@NF, all display two-phase crystalline structures of their individual two constituent phases, confirming successful preparation of the intended heterostructures. Detailed peak assignment of the four samples is shown in Table S1.†[11–14]

The high-resolution transmission electron microscopic (HR-TEM) images (Fig. 1e–g) of $NiSe/Ni_3Se_2$@NF shows two distinct lattice structures, *i.e.*, the broader lattice fringe spaces of 0.28 and 0.31 nm correspond to the (012) and (110) planes of hexagonal Ni_3Se_2, while the narrower lattice fringe spaces of 0.20 and 0.267 nm correspond to the (102) and (021) planes of hexagonal NiSe.[6,7] The HR-TEM images also reveal that Ni_3Se_2 is the dominant and skeleton phase with NiSe located at the edge of the nanorods, *i.e.*, Ni_3Se_2 nanorods wrapped by a thin NiSe layer. The HR-TEM elemental mapping (Fig. S2†) of $NiSe/Ni_3Se_2$@NF shows a uniform distribution of nickel and selenide signals. Compared with heterostructures with dissimilar cations or anions, $NiSe/Ni_3Se_2$@NF is a unique heterovalent-Ni-cation common-anion type heterostructure that is beneficial for charge transfer across the interface.

The XPS survey spectrum (Fig. S3†) of $NiSe/Ni_3Se_2$@NF shows C and O signals, aside from Ni and Se, which is attributed to the contamination/surface oxidation of the samples due to exposure to air. The high-resolution Ni 2p spectrum of $NiSe/Ni_3Se_2$@NF (Fig. 2b) reveals spin–orbital Ni^{2+} $2p_{3/2}$ and Ni^{2+} $2p_{1/2}$ peaks at 852.8 and 870.1 eV, while the higher energy peaks at 855.8 and 873.9 eV are assigned to Ni^{3+} $2p_{3/2}$ and Ni^{3+} $2p_{1/2}$, suggesting that the state of Ni in $NiSe/Ni_3Se_2$@NF is the mixed phase of Ni^{2+} and Ni^{3+}.[15,16] The peaks at 861.0 eV and 879.6 eV are assigned to the shake-up satellite peaks of Ni^{3+} $2p_{3/2}$ and Ni^{3+} $2p_{1/2}$, respectively. Besides, the high-resolution XPS spectrum of the Se 3d (Fig. 2b) consists of two peaks at binding energy of 54.84 eV and 55.74 eV, corresponding to the Se $3d_{5/2}$ and Se $3d_{3/2}$ of the metal-rich form hexagonal Ni_3Se_2 in the heterostructure. The peak at binding energy of 57.6 eV can be ascribed to the bonding structures of SeO_x, which is partial oxidation of Se under air atmosphere. The peak at binding energy of 53.8 eV belongs to hexagonal NiSe phase.[6,11,17–19] One Ni atom coordinates with 6 Se atoms and other 2 Ni atoms in NiSe; while one Ni in Ni_3Se_2 is coordinated with 4 Se and 4 Ni atoms. Ni_3Se_2 possesses more Ni–Ni bonds than NiSe, thereby exhibiting metallic conductivity. The observed lower binding energy of Ni 2p and Se 3d peaks in Ni_3Se_2 is a result of its metallic feature (Fig. 2c).[7]

Based on the above morphological and spectroscopic results, the growth and formation mechanisms of different nickel selenide coatings are proposed as follows. At the beginning of the reaction, $N_2H_4 \cdot H_2O$ assists the dissolution of Se powder to produce H^+ and Se^{2-} (eqn (1)). The resulting H^+ reacts with NF, yielding Ni^{2+} (eqn (2));[19,20] the Ni^{2+} cations and Se^{2-} anions subsequently precipitate to form the NiSe phase (eqn (3)). At a reaction temperature of 140 °C, the reaction terminates at this step, yielding pure NiSe coating on NF, *i.e.*, NiSe@NF. At elevated hydrothermal temperature of 200 °C, Ni^{2+} can be reduced by hydrazine hydrate to reactive $Ni^{\bullet}$ atoms (eqn (4)) upon heating, which further reacts with NiSe to form Ni_3Se_2 (eqn (5)) under hydrothermal conditions.[7,12] At a low dosage of Se powder, pure Ni_3Se_2 coating on nickel foam is formed, *i.e.*, Ni_3Se_2@NF. At higher Se dosage, NiSe continues to form on the surface of Ni_3Se_2, leading to the formation of heterostructured $NiSe/Ni_3Se_2$@NF. To sum up, the formation of different Ni selenide coatings on NF is a combined consequence of hydrothermal reaction temperature and Se usage. The XRD, SEM and HR-TEM results agree well with the above proposed reaction mechanisms.

$$N_2H_4 \cdot H_2O + Se \rightarrow 4H^+ + Se^{2-} + N_2\uparrow + H_2O \quad (1)$$

$$2H^+ + Ni \rightarrow Ni^{2+} + H_2 \quad (2)$$

$$Ni^{2+} + Se^{2-} \rightarrow NiSe \quad (3)$$

$$Ni^{2+} + N_2H_4 \cdot H_2O \rightarrow Ni^{\bullet} + N_2 + 2H_2 + H_2O \quad (4)$$

$$2NiSe + Ni^{\bullet} \rightarrow Ni_3Se_2 \quad (5)$$

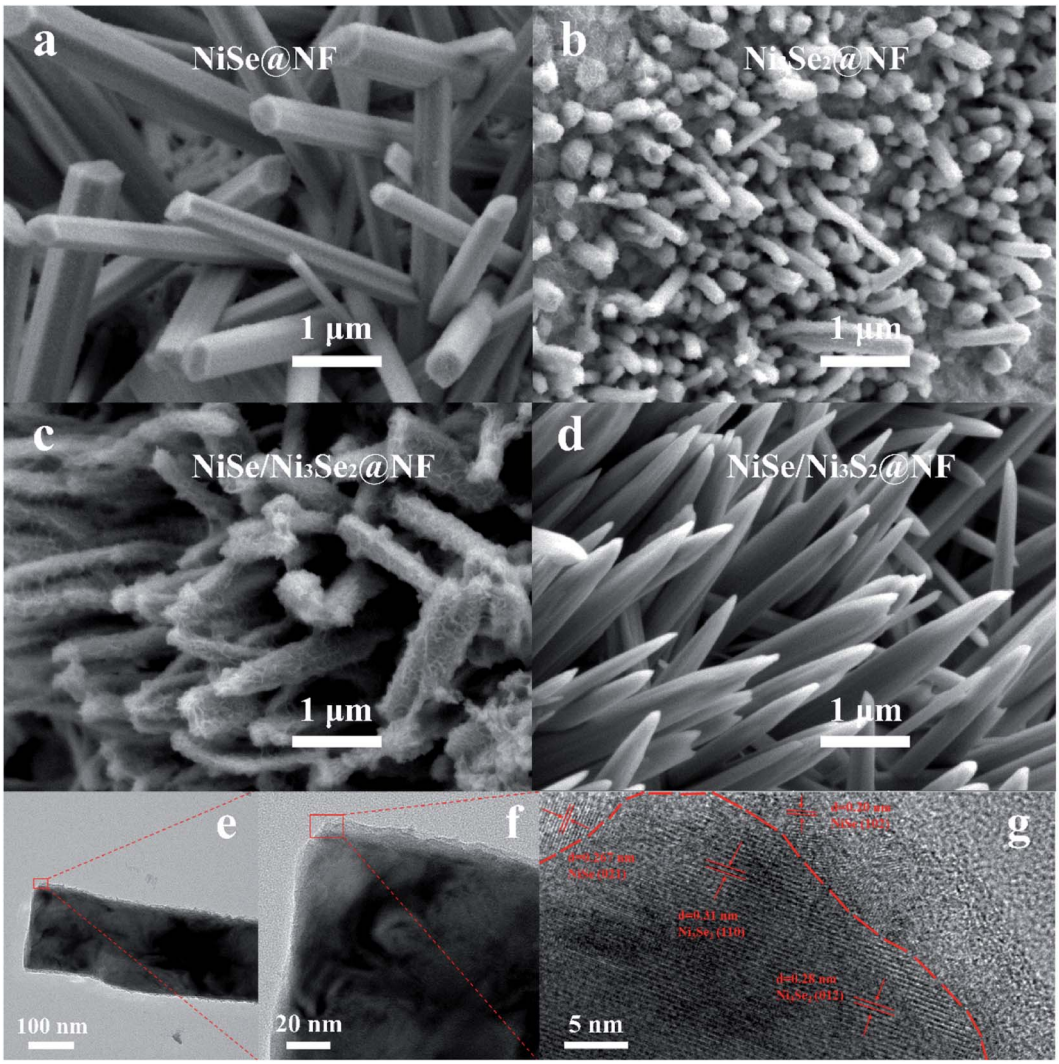

Fig. 1 Morphological and structural characterizations. SEM images of NiSe@NF (a) Ni_3Se_2@NF (b) NiSe/Ni_3Se_2@NF (c) NiSe/Ni_3S_2@NF (d) and high-resolution TEM images of NiSe/Ni_3Se_2@NF (e–g).

The HER catalytic behaviors of all samples were evaluated and compared with bare NF and Pt/C@NF in a standard three-electrode electrochemical cell using 1.0 M KOH aqueous solution. The linear sweep voltammograms (LSV, Fig. 3a) show that all the samples exhibit HER catalytic behaviors, with more positive onset potentials and higher cathodic currents than bare NF, suggesting that nickel selenides generally have higher HER catalytic activities than nickel metal. Among all the four

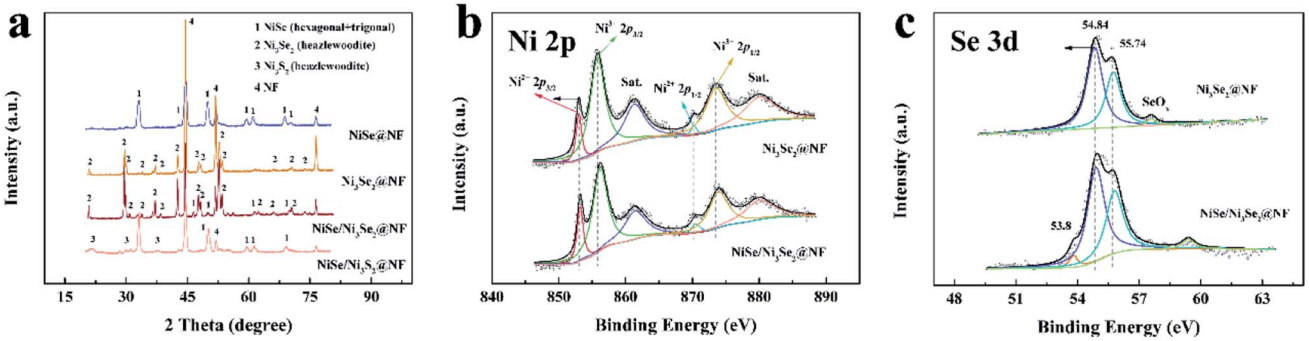

Fig. 2 Spectroscopic characterizations. XRD patterns (a) of Ni_3Se_2@NF, NiSe@NF, NiSe/Ni_3Se_2@NF, and NiSe/Ni_3S_2@NF. (b) Ni 2p spectra. (c) XPS fitting of Se 3d peaks of NiSe/Ni_3Se_2@NF and Ni_3Se_2@NF.

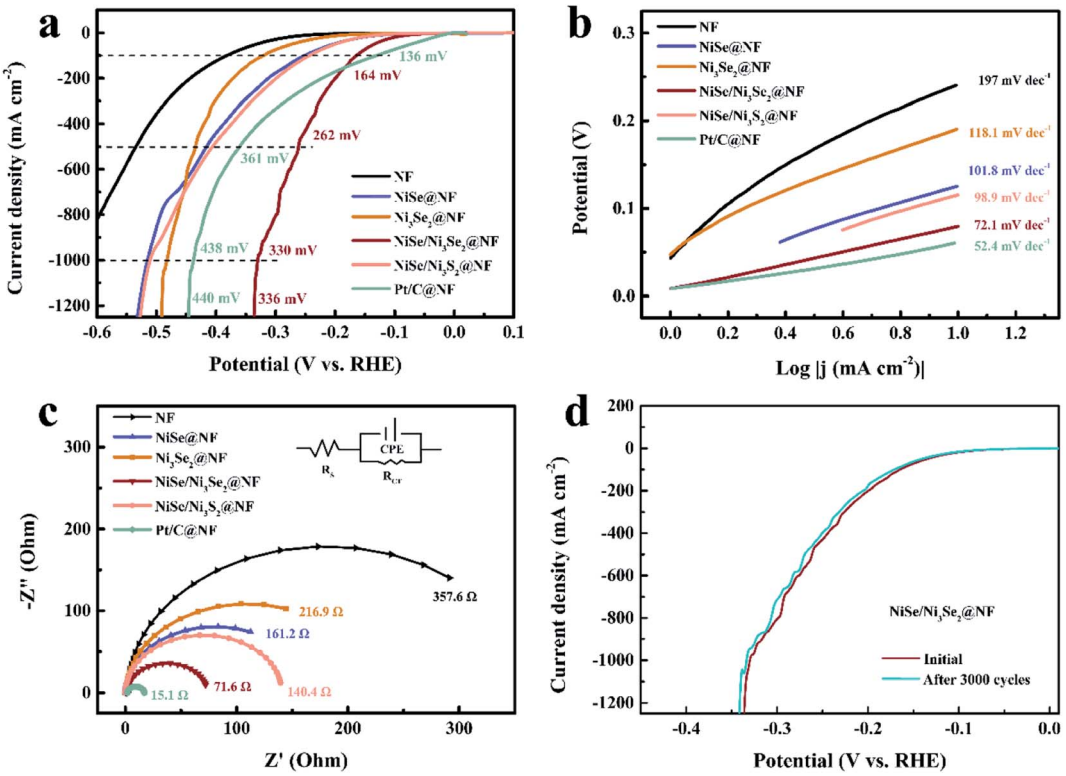

Fig. 3 HER activity and stability of the various electrocatalyst. (a) Linear sweep voltammetry polarization curves of NF, Ni_3Se_2@NF, NiSe@NF, NiSe/Ni_3Se_2@NF, NiSe/Ni_3S_2@NF, and Pt/C@NF electrocatalysts in 1.0 M KOH solution. (b) Tafel plots obtained from the LSV curves in (a). (c) Nyquist plots of the above electrocatalysts in 1.0 M KOH with frequency values ranging from 0.01 Hz to 10^5 Hz. (d) Polarization curves of NiSe/Ni_3Se_2@NFrecorded at the initial and the 3000th potential cycles in 1.0 M KOH.

selenide samples, NiSe/Ni_3Se_2@NF shows the best electrocatalytic performance as evidenced by its lowest overpotential and highest cathodic current density. Compared with Pt/C@NF, the HER onset potential of NiSe/Ni_3Se_2@NF is 50 mV more negative. At low current density of 10 mA cm^{-2}, NiSe/Ni_3Se_2@NF also shows an overpotential that is 61 mV higher than Pt/C (Fig. S4†), but their LSV curves intersect with each other at current density of 180 mA cm^{-2}. At higher current beyond the intersection (>180 mA cm^{-2}), NiSe/Ni_3Se_2@NF requires lower overpotentials than Pt/C@NF to deliver the same current density. To reach ultra-high current densities of 500, 1000 and 1250 mA cm^{-2}, NiSe/Ni_3Se_2@NF only requires overpotentials of 262, 330 and 336 mV, respectively, outperforming Pt/C@NF (η_{500}, η_{1000} and η_{1250} = 351, 438 and 440 mV) for high-rate HER. Among all the selenide samples, NiSe/Ni_3Se_2@NF also displays the lowest Tafel slope of 72.1 mV dec^{-1} (Fig. 4b), indicating that the HER occurs *via* the Volmer–Heyrovsky mechanism with the Volmer step (water discharge) as the bottleneck. The Vomer-step-determined alkaline HER requires fast water dissociation and appropriate adsorption of H_{ad}/OH_{ad}.[21] In this sense, heterostructured electrocatalysts are generally more prone to meeting the multiple requirements through their multiple active sites and electronic structure modulation.[22,23]

The charge transfer and ion diffusion properties of different electrodes were studied by electrochemical impedance spectroscopy (EIS) and electrochemical active surface area (ECSA). The fitted Nyquist plots (Fig. 3c and Table S2†) show that NiSe/Ni_3Se_2@NF has the lowest charge-transfer resistance (R_{CT}) value of 71.6 Ω among all the selenide samples. The low R_{CT} value and Tafel slope of NiSe/Ni_3Se_2@NF are both beneficial to its catalytic performances, particularly at high current densities. The ECSA values as derived from the electrochemical double-layer capacitance (C_{dl}) are plotted in Fig. S5.† NiSe/Ni_3Se_2@NF displays the highest C_{dl} value of 25.17 mF cm^{-2} among all the selenide samples, indicating the highest number of active sites on NiSe/Ni_3Se_2@NF. The high C_{dl} value agrees well with the SEM observation (Fig. 2) that the nanorods of NiSe/Ni_3Se_2@NF have rougher surface than the other samples. The charge density difference plots (Fig. S6†) also reveal electron enrichment at the interface between NiSe and Ni_3Se_2. This finding suggests the interfacial region can probably provide additional HER active sites, complementing to the two known optimal sites, *i.e.*, Se on NiSe and Ni on Ni_3Se_2.[6,7] As a result of the additional active sites and the higher ECSA, NiSe/Ni_3Se_2@NF shows a much higher exchange current density (j_0, Table S3†) than the other selenide samples.

The stability of NiSe/Ni_3Se_2@NF was evaluated by the chronoamperometric test, which demonstrates ultra-high durability as evidenced by the nearly overlapped LSV curve after 3000 CV cycles (Fig. 3d). The stability is further verified by the 30 h potentiostatic HER test. At η = 164 mV, a constant current density of 100 mA cm^{-2} is maintained after 30 h; while at η =

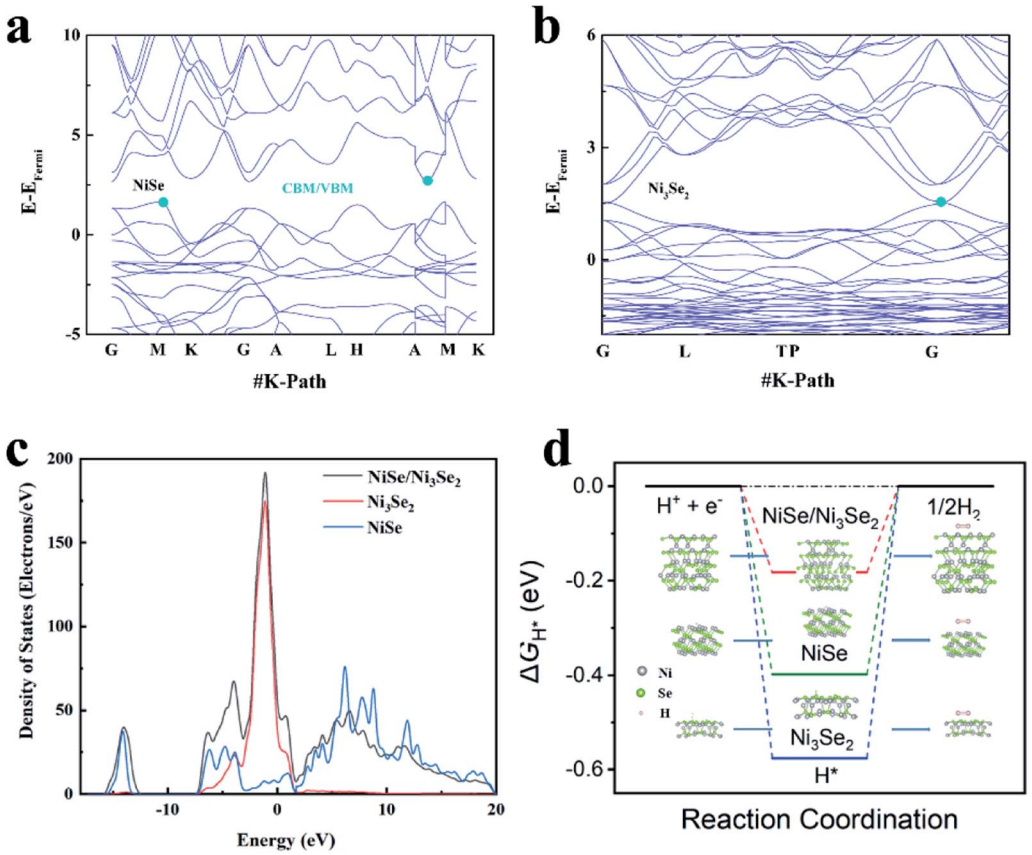

Fig. 4 Computed band structures of NiSe (a) and Ni_3Se_2 (b), computed density of states (DOS) (c) and ΔG_H (d) of NiSe, Ni_3Se_2 and NiSe/Ni_3Se_2.

164 mV, NiSe/Ni_3Se_2@NF shows fairly slow decrease of current density (Fig. S7†). The amount of H_2 gas produced by NiSe/Ni_3Se_2@NF is exactly the same as the theoretical value during galvanostatic HER in 2 h (Fig. S8†), suggesting a nearly 100% faradaic efficiency. The SEM images (Fig. S9†), XRD pattern (Fig. S10†) and the XPS spectra (Fig. S11†) indicate that the NiSe/Ni_3Se_2@NF electrocatalyst undergo no morphological, structural or chemical change after 3000 CV cycles. The superior stability of NiSe/Ni_3Se_2@NF is attributed to its intrinsic chemical stability, as well as the robust mechanical properties resulting from the *in situ* growth of the selenide coating on NF.[10,24]

To gain further insight into the heterostructure features, Mott–Schottky (M–S) analysis was performed at an AC frequency of 1 kHz. The M–S diagram (Fig. S12†) exhibits positive slope of n-type semiconductor properties.[25,26] A recent work demonstrates that n-type semiconductor electrocatalysts favor cathodic reactions such as HER because of their self-gating under negative electrode potentials.[27] All the selenide samples belong to the n-type, so they are promising HER electrocatalysts from this perspective. DFT calculations (structural model shown in Fig. S13†) shows that NiSe and Ni_3Se_2 possess different band structures (Fig. 4a and b). NiSe shows a clear gap between its valence and conduction band (VB and CB), while the VB and CB of Ni_3Se_2 shows overlap, suggesting that NiSe is a typical semiconductor but Ni_3Se_2 exhibits metallic-type conductivity. Therefore, the electric conductivity in NiSe/Ni_3Se_2@NF follows NF > Ni_3Se_2 > NiSe. This descending order of conductivity from substrate to the electrode surface is in accordance with the rational design principle of electrocatalyst with rapid charge transfer properties.[10] The calculated density of states (DOS, Fig. 4c) suggest that the DOS of NiSe/Ni_3Se_2 below the Fermi level is mainly contributed by Ni_3Se_2, while above the Fermi level is jointly contributed by NiSe to a large extent. The DOS results also indicate that the electrical properties of heterojunction, especially the width of valence band, are significantly larger than that of the single component. Therefore, the two components in the heterojunction have strong hybridization. The electronic structure modulation is further verified by the free energy with hydrogen (ΔG_H), as illustrated in Fig. 4d. The computed hydrogen adsorption free energy (ΔG_{H^*}) of NiSe/Ni_3Se_2 is the lowest among all the three electrocatalysts. High HER catalytic activity generally requires a ΔG_{H^*} value close to 0 eV because it offers both moderate H chemisorption and releasing strength.[31] The more negative ΔG_{H^*} values of NiSe and Ni_3Se_2 indicates lower HER catalytic activities, which can be attributed to the formation of NiH_{ads} species ($Ni + H^+ + e^- \rightarrow NiH_{ads}$) and SeH_{ads} species ($Se + H^+ + e^- \rightarrow SeH_{ads}$) with strong binding energy during the Volmer reaction in HER processes, respectively.[32,33] The near-zero ΔG_{H^*} value of the NiSe/Ni_3Se_2 structure is an indication of its optimal adsorption and dissociation ability for H*, in agreement with the observed higher exchange current density (j_0, Table S3†).

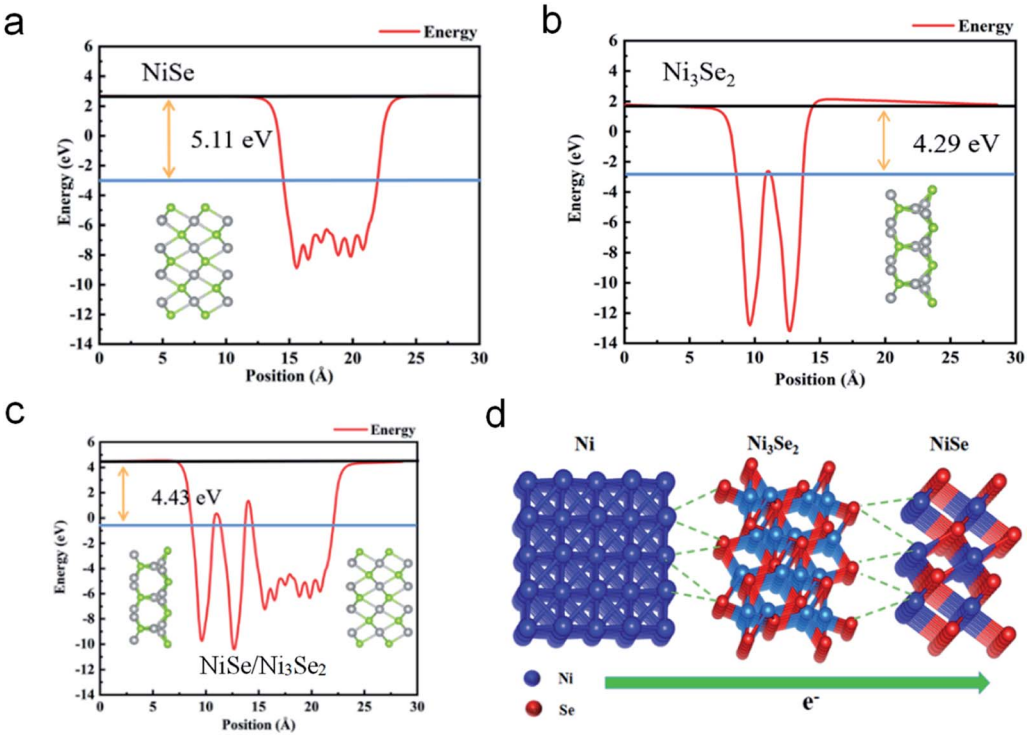

Fig. 5 Computed work function of NiSe (a), Ni_3Se_2 (b) and NiSe/Ni_3Se_2 (c), and illustration of the electron transfer in NiSe/Ni_3Se_2@NF (d), the dashed lines in (d) represent Ni–Se bonds between Ni and Ni_3Se_2, and between Ni_3Se_2 and NiSe.

Aside from the higher conductivity and electron density, Ni_3Se_2 has lower work function than NiSe (Fig. 5a and b). The lower work function of Ni_3Se_2 is in agreement with previous theoretical work,[28] which attributes this to the lower oxidation state and lower electronegativity of Ni atoms in Ni_3Se_2 than NiSe. In the NiSe/Ni_3Se_2 heterojunction, a built-in electric field (BIEF) is formed which induces electron injection from the lower to higher work function material,[29] *i.e.*, electron transfer from Ni_3Se_2 to NiSe. This BIEF originates from the band alignment in order to achieve a work function equilibrium (Fig. 5c) between NiSe and Ni_3Se_2. The charge density difference plots (Fig. S6†) also show that the electron density is reduced on Ni_3Se_2 but increased on NiSe upon contact, confirming the spontaneous electron transfer from Ni_3Se_2 to NiSe. The resulting BIEF facilitates unidirectional interfacial charge transfer that is in line with the cathodic current flow (Fig. 5d) and hence enhances the HER catalytic activity.[30,34] Furthermore, NiSe/Ni_3Se_2 belongs to a unique type of common-anion heterovalent-common-cation heterojunction, which possesses ample Ni–Se bonds (Fig. 5d) across the interface to reduce the interfacial charge transfer resistance. In fact, NiSe and Ni_3Se_2 have similar lattice parameters,[35] so the lattice mismatch in the NiSe/Ni_3Se_2 heterostructure is small, also beneficial for interfacial Ni–Se bonds and charge transfer. The dissimilar-anion heterostructured NiSe/Ni_3S_2@NF exhibits higher overpotentials (Fig. 3a) and higher charge transfer resistance (Fig. 3c) than NiSe/Ni_3Se_2@NF, confirming that the common-anion feature is favorable for HER electrocatalysis.

Coupled with the experimental results and the theoretical analysis, the superior high-rate HER performance of NiSe/Ni_3Se_2@NF is rationalized as follows. (1) The nanorod-array morphology and high surface roughness affords high surface area and exposure of catalytic active sites. (2) The multiple active sites and electronic structure modulation in the heterostructure meet the specific requirements of the elementary steps of alkaline HER. (3) The hydrophilic and aerophobic surface originating from the micro-architecture is beneficial for mass transfer at high reaction rates. (4) The common-anion heterostructure presents ample interfacial Ni–Se bonds to facilitates charge transfer across the interface. (5) The different electronegativity of Ni cations results in a built-in electric field that induces spontaneous electron transfer from Ni_3Se_2 to NiSe. The observed low onset potential of NiSe/Ni_3Se_2@NF is attributed to standpoint (1) and (2), whereas its superior high-rate HER performance is mainly due to (3), (4) and (5).

Conclusions

In conclusion, we report one-step hydrothermal synthesis of NiSe/Ni_3Se_2@NF heterostructure through control of reaction temperature and reactant molar ratio. This common-anion heterovalent-common-cation heterostructure shows superior catalytic performances in ultra-high-rate alkaline HER. The morphological features offer high number of active sites and the heterostructure provides multiples catalytic sites and electronic structure modulation. Moreover, the rationally designed NiSe/Ni_3Se_2@NF results in built-in electric field and efficient

interfacial charge transfer, both responsible for its excellent high-rate HER performances.

Conflicts of interest

The authors declare no competing financial interest.

Acknowledgements

This work received financial support from the Science and Technology Bureau of Shenzhen (Grant No. JCYJ20170306171540744).

References

1 N. Armaroli and V. Balzani, The hydrogen issue, *ChemSusChem*, 2011, **4**, 21–36.
2 I. Dincer and C. Acar, Smart energy solutions with hydrogen options, *Int. J. Hydrogen Energy*, 2018, **43**, 8579–8599.
3 B. Yu, Y. Hu, F. Qi, X. Wang, B. Zheng, K. Liu, W. Zhang, Y. Li and Y. Chen, Nanocrystalline $Ni_{0.85}Se$ as efficient non-noble-metal electrocatalyst for hydrogen evolution reaction, *Electrochim. Acta*, 2017, **242**, 25–30.
4 G. Li, J. Yu, J. Jia, L. Yang, L. Zhao, W. Zhou and H. Liu, Cobalt-Cobalt phosphide nanoparticles@nitrogen-phosphorus doped carbon/graphene derived from cobalt ions adsorbed saccharomycete yeasts as an efficient, stable, and large-current-density electrode for hydrogen evolution reactions, *Adv. Funct. Mater.*, 2018, **28**, 1801332.
5 C. Tang, Z. Pu, Q. Liu, A. M. Asiri, X. Sun, Y. Luo and Y. He, In situ growth of NiSe nanowire film on nickel foam as an electrode for high-performance supercapacitors, *ChemElectroChem*, 2015, **2**, 1903–1907.
6 Y. Zhong, B. Chang, Y. Shao, C. Xu, Y. Wu and X. Hao, Regulating phase conversion from Ni_3Se_2 to NiSe in bifunctional electrocatalyst for overall water splitting enhancement, *ChemSusChem*, 2019, **12**, 2008–2014.
7 H.-B. Wang, Y.-S. Sun, F. Ma, L. Zhou, H.-F. Li, L. Zhang, G.-J. Chen, Y.-K. Xu, Y.-N. Chen, K.-W. Xu and D.-Y. Ma, Se molarity tuned composition and configuration of Ni_3Se_2/NiSe core-shell nanowire heterostructures for hydrogen evolution reaction, *J. Alloys Compd.*, 2020, **819**, 153056.
8 X. Wang, X. Wang, J. Huang, S. Li, A. Meng and Z. Li, Interfacial chemical bond and internal electric field modulated Z-scheme S_v-$ZnIn_2S_4$/$MoSe_2$ photocatalyst for efficient hydrogen evolution, *Nat. Commun.*, 2021, **12**, 4112.
9 Y. Liao, K. Pan, Q. Pan, G. Wang, W. Zhou and H. Fu, In situ synthesis of a NiS/Ni_3S_2 nanorod composite array on Ni foil as a FTO-free counter electrode for dye-sensitized solar cells, *Nanoscale*, 2015, **7**, 1623–1626.
10 X. Ma, W. Chen, Q. Li, L. Xue and C. Peng, Nitrogen-doped hierarchical heterostructured aerophobic MoS_x/Ni_3S_2 nanowires by one-pot synthesis: system engineering and synergistic effect in electrocatalysis of hydrogen evolution reaction, *Energy Environ. Mater.*, 2020, 1.
11 Y. Tian, Y. Ruan, J. Zhang, Z. Yang, J. Jiang and C. Wang, Controllable growth of NiSe nanorod arrays via one-pot hydrothermal method for high areal-capacitance supercapacitors, *Electrochim. Acta*, 2017, **250**, 327–334.
12 X. Zhang, M. Zhen, J. Bai, S. Jin and L. Liu, Efficient NiSe-Ni_3Se_2/graphene electrocatalyst in dye-sensitized solar cells: the role of hollow hybrid nanostructure, *ACS Appl. Mater. Interfaces*, 2016, **8**, 17187–17193.
13 F. Zhang, Y. Pei, Y. Ge, H. Chu, S. Craig, P. Dong, J. Cao, P. M. Ajayan, M. Ye and J. Shen, Controlled synthesis of eutectic NiSe/Ni_3Se_2 self-supported on Ni foam: an excellent bifunctional electrocatalyst for overall water splitting, *Adv. Mater. Interfaces*, 2018, **5**, 1701507.
14 Z. Zou, X. Wang, J. Huang, Z. Wu and F. Gao, An Fe-doped nickel selenide nanorod/nanosheet hierarchical array for efficient overall water splitting, *J. Mater. Chem. A*, 2019, **7**, 2233–2241.
15 J. Zhang, Y. Li, T. Zhu, Y. Wang, J. Cui, J. Wu, H. Xu, X. Shu, Y. Qin, H. Zheng, P. M. Ajayan, Y. Zhang and Y. Wu, 3D coral-like Ni_3S_2 on Ni foam as a bifunctional electrocatalyst for overall water splitting, *ACS Appl. Mater. Interfaces*, 2018, **10**, 31330–31339.
16 C. Tang, N. Cheng, Z. Pu, W. Xing and X. Sun, NiSe nanowire film supported on nickel foam: an efficient and stable 3D bifunctional electrode for full water splitting, *Angew. Chem., Int. Ed.*, 2015, **54**, 9351–9355.
17 H. Li, S. Chen, H. Lin, X. Xu, H. Yang, L. Song and X. Wang, Nickel diselenide ultrathin nanowires decorated with amorphous nickel oxide nanoparticles for enhanced water splitting electrocatalysis, *Small*, 2017, **13**, 1701487.
18 X. Yu, W. Sun and Y. Chu, One-pot solvothermal synthesis and properties of 1D NiSe and NiSe-Ni_3S_2 alloyed compound nanorod arrays, *New J. Chem.*, 2014, **38**, 70–76.
19 C. Bao, F. Li, J. Wang, P. Sun, N. Huang, Y. Sun, L. Fang, L. Wang and X. Sun, One-pot solvothermal in situ growth of 1D single-crystalline NiSe on Ni foil as efficient and stable transparent conductive oxide free counter electrodes for dye-sensitized solar cells, *ACS Appl. Mater. Interfaces*, 2016, **8**, 32788–32796.
20 L. Zhang, J. C. Yu, M. Mo, L. Wu, Q. Li and K. W. Kwong, A general solution-phase approach to oriented nanostructured films of metal chalcogenides on metal foils: the case of nickel sulfide, *J. Am. Chem. Soc.*, 2004, **126**, 8116.
21 L. Zhao, Y. Zhang, Z. Zhao, Q.-H. Zhang, L.-B. Huang, L. Gu, G. Lu, J.-S. Hu and L.-J. Wan, Steering elementary steps towards efficient alkaline hydrogen evolution via size-dependent Ni/NiO nanoscale heterosurfaces, *Natl. Sci. Rev.*, 2020, **7**, 27–36.
22 Y. Jiang, P. Sun, L. Sharma, B. Mao, R. Kakkar, T. Meng, L. Zheng and M. Cao, Further insights into bifunctional mechanism in alkaline hydrogen evolution for hybridized nanocatalysts and general route toward mechanism-oriented synthesis, *Nano Energy*, 2021, **81**, 105645.
23 J. Ge, J. Jin, Y. Cao, M. Jiang, F. Zhang, H. Guo and X. Lei, Heterostructure Ni_3S_4-MoS_2 with interfacial electron redistribution used for enhancing hydrogen evolution, *RSC Adv.*, 2021, **11**, 19630–19638.
24 X. Liu, S. Li, B. Akinwolemiwa, D. Hu, T. Wu and C. Peng, Low-crystalline transition metal oxide/hydroxide on

MWCNT by Fenton-reaction-inspired green synthesis for lithium ion battery and OER electrocatalysis, *Electrochim. Acta*, 2021, **387**, 138559.

25 S. Bolar, S. Shit, J. S. Kumar, N. C. Murmu, R. S. Ganesh, H. Inokawa and T. Kuila, Optimization of active surface area of flower like MoS_2 using V-doping towards enhanced hydrogen evolution reaction in acidic and basic medium, *Appl. Catal., B*, 2019, **254**, 432–442.

26 D. He, L. Cao, Y. Huang, G. Li, Y. Feng, Y. Zhao, X. Li, D. Li and L. Feng, Tuning the morphologic and electronic structures of self-assembled $NiSe/Ni_3Se_2$ heterostructures with vanadium doping toward efficient electrocatalytic hydrogen, *Appl. Surf. Sci.*, 2021, **542**, 148598.

27 Y. He, et al., Self-gating in semiconductor electrocatalysis, *Nat. Mater.*, 2019, **18**, 1098–1104.

28 M. T. Greiner, L. Chai, M. G. Helander, W.-M. Tang and Z.-H. Lu, Transition metal oxide work functions: the influence of cation oxidation state and oxygen vacancies, *Adv. Funct. Mater.*, 2012, **22**, 4557–4568.

29 Z. Li, Y. Pei, R. Ma, Y. Wang, Y. Zhu, M. Yang and J. Wang, A phosphate semiconductor-induced built-in electric field boosts electron enrichment for electrocatalytic hydrogen evolution in alkaline conditions, *J. Mater. Chem. A*, 2021, **9**, 13109–13114.

30 M. S. Hassan, P. Basera, S. Gahlawat, P. P. Ingole, S. Bhattacharya and S. Sapra, Understanding the efficient electrocatalytic activities of $MoSe_2$-Cu_2S nanoheterostructures, *J. Mater. Chem. A*, 2021, **9**, 9837–9848.

31 Z. Pu, J. Zhao, I. S. Amiinu, W. Li, M. Wang, D. He and S. Mu, A universal synthesis strategy for P-rich noble metal diphosphide-based electrocatalysts for the hydrogen evolution reaction, *Energy Environ. Sci.*, 2019, **12**, 952–957.

32 Y. Zheng, Y. Jiao, M. Jaroniec and S. Z. Qiao, Advancing the Electrochemistry of the Hydrogen-Evolution Reaction through Combining Experiment and Theory, *Angew. Chem., Int. Ed.*, 2015, **54**, 52–65.

33 Y. Liang, Y. Li, H. Wang, J. Zhou, J. Wang, T. Regier and H. Dai, Co_3O_4 Nanocrystals on Graphene as a Synergistic Catalyst for Oxygen Reduction Reaction, *Nat. Mater.*, 2011, **10**, 780.

34 Z. Niu, C. Qiu, J. Jiang and L. Ai, Hierarchical CoP-FeP branched heterostructures for highly efficient electrocatalytic water splitting, *ACS Sustainable Chem. Eng.*, 2018, **7**, 2335–2342.

35 K. Unoki, A. Yoshiasa, G. Kitahara, T. Nishiayama, M. Tokuda, K. Sugiyama and A. Nakatsuka, Crystal structure refinements of stoichiometric Ni_3Se_2 and NiSe, *Acta Crystallogr., Sect. C: Struct. Chem.*, 2021, **77**, 169–175.